

The Structure and Dark Halo Core Properties of Dwarf Spheroidal Galaxies

A. Burkert^{1,2}

burkert@usm.uni-muenchen.de

ABSTRACT

The structure and dark matter halo core properties of dwarf spheroidal galaxies (dSphs) are investigated. A double-isothermal (DIS) model of an isothermal, non self-gravitating stellar system, in gravitational equilibrium and embedded in an isothermal dark halo core provides an excellent fit to the various observed stellar surface density distributions $\Sigma_*(r)$. Despite its constant velocity dispersion, the stellar system can be well characterised by King profiles (King 1966) with a broad distribution of concentration parameters $c = \log(r_{*,t}/r_{*,c})$, with $r_{*,t}$ and $r_{*,c}$ the stellar tidal and core radius, respectively. The DIS model confirms the suggestion of Kormendy & Freeman (2014) that the core scale length of the stellar system, defined as $a_* = -(d \ln \Sigma_*/dr^2)^{-1/2}$, is sensitive to the central dark matter density ρ_0 . In contrast to single-component systems, $r_{*,t}$ however does not trace the tidal radius of the galaxy but the core radius r_c of its dark matter halo. c is therefore sensitive to the ratio σ_*/σ_0 with σ_* and σ_0 the stellar and dark matter velocity dispersion, respectively. Simple empirical relationships are derived that allow to calculate the dark halo core parameters ρ_0 , r_c and σ_0 , given the observable quantities σ_* , a_* and c . The DIS model is applied to the Milky Way's dSphs. Their halo velocity dispersions lie in a narrow range of $10 \text{ km/s} \leq \sigma_0 \leq 18 \text{ km/s}$ with halo core radii of $280 \text{ pc} \leq r_c \leq 1.3 \text{ kpc}$ and $r_c \approx 2a_*$. All dSphs follow closely the same universal scaling relations $\langle \rho_0 r_c \rangle \equiv \rho_0 \times r_c = 75^{+85}_{-45} \text{ M}_\odot \text{ pc}^{-2}$ and $\sigma_0^2 \times r_c^{-1} = 0.45^{+0.51}_{-0.27} (\text{km/s})^2 \text{ pc}^{-1}$ that characterise the cores of more massive galaxies over a range of 18 magnitudes in blue magnitude M_B . For given $\langle \rho_0 r_c \rangle$ the core mass is a strong function of core radius, $M_c \sim r_c^2$. Inside a fixed radius r_u , with r_u the logarithmic mean of the dSph's core radii, the total mass $M_u = 2.17 \langle \rho_0 r_c \rangle r_u^2$ is however roughly constant. Outliers with smaller masses are expected for dSphs with core radii that are much larger or smaller than r_u . For the Milky Way's dSphs we find $r_u = 400 \pm 100 \text{ pc}$ and $M_u = 2.6 \pm 1.4 \times 10^7 \text{ M}_\odot$, in agreement with Strigari et al. (2008). Due to their small r_c , the core densities of the Galaxy's dSphs are very higher, with $\rho_0 = 0.03 - 0.3 \text{ M}_\odot \text{ pc}^{-3}$. The dSphs would have to be on galactic orbits with pericenters smaller than a few kpc in order for their stellar systems to be affected by Galactic tides which is very unlikely. dSphs should therefore be tidally undisturbed. Observational evidence for tidal effects might then provide a serious challenge for the cold dark matter scenario.

¹University Observatory Munich (USM), Scheinerstrasse 1, 81679 Munich, Germany

²Max-Planck-Fellow, MPE Garching, Germany

Subject headings: dark matter – galaxies: dwarf – galaxies:formation – galaxies: kinematics – galaxies: structure

1. Introduction

The nature of dark matter is still a mystery. Standard cosmology works with the assumption of a massive, weakly and gravitationally interacting particle (e.g. White 1982; Steigman & Turner 1985; Jungman et al. 1996). This cold dark matter (CDM) scenario has proven to be very successful on large galactic and extragalactic scales, from cosmic structure formation to the outer rotation curves of galaxies and the stability of galactic disks (Ostriker & Peebles 1973). The success of the CDM model however is also to some extent frustrating as any additional physical properties of the CDM particle remain hidden. Scientists are therefore searching for failures of CDM predictions that might lead to new insight into the nature and origin of the dark matter particle.

Several small-scale problems of the CDM model have been discussed in the literature. These include the distribution of satellite galaxies in large planar structures (e.g. Kroupa 2005; Ibata et al. 2013; Goerdt et al. 2014) or the mass-luminosity problem of satellite galaxies (Kroupa 2010). One of the most prominent such failures is the cusp-core problem (e.g. Moore 1994; Flores & Primack 1994; Burkert 1995; Strigari et al. 2008; Primack 2009; de Blok 2010; Boylan-Kochlin et al. 2011; Ogiya & Mori 2014; Ogiya et al. 2014; Ogiya & Burkert 2015). While simulations predict cuspy central density profiles of CDM halos with the density increasing steeply towards the center (Dubinski & Carlberg 1991; Navarro et al. 1997; Moore et al. 1999; Dekel et al. 2003), observations often indicate a flat dark matter density core (e.g. Flores & Primack 1994; Moore 1994; Burkert 1995; de Blok et al. 2008; Gentile et al. 2009; Oh et al. 2011). The cusp-core problem is best documented in low-mass dwarf galaxies which are characterised by low baryon fractions and which therefore are ideal tracers of the underlying dark halo structure, unperturbed by the gravitational influence of the baryonic component. In addition, dwarf galaxies appear to host the highest density dark matter cores, making an analysis of the halo structure easier.

Ideally one would like to investigate $H\alpha$ /HI rotation curves (e.g. Carignan & Freeman 1985; de Blok et al. 2001; Corbelli et al. 2014) which are a clear tracer of the gravitational potential as function of radius. One of the problems however is that for low-mass galaxies the stellar- and gas velocity dispersions begin to exceed their rotational velocity. This is especially true for one of the smallest galaxies, known as dwarf spheroidals (dSph), the target of this paper. Recently, Kormendy & Freeman (KF14; 2014) investigated the dark halo scaling laws in late-type galaxies, including dSphs (see also Burkert 1997; Salucci et al. 2012). Interestingly, the stellar velocity dispersion σ_* of the dSphs is of order 8-10 km/s, very similar to the universal turbulent velocity of the diffuse gas component in most low-redshift star forming disk galaxies (Dib et al. 2006). However, in contrast to more massive galaxies, the gravitational field in dSphs is small, generating rotation curves of order $v_{rot} \approx 10$ km/s (see section 4). Even if the star forming gas would have had enough angular momentum to settle initially into a thin disk configuration, stellar feedback

processes could easily destroy the disk, ejecting gas in a wind and leading to a dispersion-dominated spheroidal stellar system (Navarro et al. 1996; Maller & Dekel 2002; Teyssier et al. 2013).

KF14 consider a spherically symmetric stellar system with constant σ_* , embedded in a spherically symmetric dark matter core with constant density ρ_0 . Solving the hydrostatic equation (see equation 3) and assuming that the stellar system is not self-gravitating they find that the stellar density distribution should be a Gaussian

$$\rho_*(r) = \rho_{*,0} \times \exp\left(-\frac{r^2}{a_*^2}\right) \quad (1)$$

with $\rho_{*,0} = \rho_*(r=0)$ the central stellar density and

$$a_* = \left(\frac{3\sigma_*^2}{2\pi G\rho_0}\right)^{1/2} \quad (2)$$

the scale length of the stellar system. The projected surface density distribution Σ_* in this case is also a Gaussian with the same scale length. Remarkably, KF14 show that many dSphs follow a Gaussian stellar surface density distribution better than the typical exponential profile, seen for galactic disks.

KF14 however also find that some dSphs cannot be fitted by a Gaussian. In addition, also dSphs with inner Gaussian slopes show deviations further out. Another problem is the fact that isothermal, isotropic dark matter cores in equilibrium cannot have precisely constant densities, requiring a more detailed investigation. Finally, equation 2 does not provide any information about the dark halo core radii, velocity dispersions and masses. KF14 shift the observed stellar scale length a_* and velocity dispersion σ_* along lines of constant ρ_0 onto the core scaling relations of more massive galaxies, in order to infer the halo core properties. It is however not clear whether dSphs should follow the same core scaling relations as more massive galaxies.

In this paper we therefore have a more detailed look at the coupled kinematics of stars and dark matter in dSphs, relaxing the assumption of a constant density dark matter core. Section 2 solves the hydrostatic equation of two isothermal particle systems, coupled by their joint gravitational field. We derive formulas on how to determine the dark matter core density and how to shift the observed stellar velocity dispersion σ_* and central stellar scale length a_* in order to infer the dark halo velocity dispersion σ_0 and halo core radius r_c . Section 3 then focusses on deviations from Gaussian profiles and the origin of King profiles in isothermal dSphs. This section demonstrates that the King concentration parameter c is tightly related to the dark halo velocity dispersion and by this also makes it possible to determine the halo core radius and core mass. These analytical results are then applied to the Milky Way’s system of dSphs in section 4 to investigate their halo core properties. Section 5 discusses the conjecture of Strigari et al. (2008) that dSphs have a universal mass, of order $10^7 M_\odot$, within a scale radius of 300 pc. Section 6 summarises the results

and concludes.

2. The structure of double-isothermal (DIS) particle systems

We assume that the cores of dark matter halos in dSphs are isothermal and isotropic with a constant velocity dispersion σ_0 . This assumption certainly has to break down at some point as otherwise the dark halo mass would diverge as $M(r) \sim r$. For investigations of the outer halo regions, the Burkert profile (Burkert 1995) might therefore provide a better approximation. It combines an isothermal-like inner core with the characteristic r^{-3} outer density decline, seen in most CDM simulations.

Observations also indicate that the main stellar body of dSphs is characterised by an almost constant velocity dispersion σ_* , well beyond the half-light radius (Walker et al. 2009; Salucci et al. 2012, KF14). Majewski et al. (2013) recently reported a drop in σ_* in the heart of the Sagittarius dwarf spheroidal galaxy. This feature is however limited to the very center that is small compared the half-light radius. A central decline in σ_* might in fact be a characteristic property of dSphs in general. Many of them show a strong increase in stellar surface density in the very center, requiring a change in their kinematics, most likely a declining velocity dispersion, in order to be in hydrostatic equilibrium. The origin of cold nuclei in dSphs is certainly an interesting and yet unsolved problem. Here, however, we are interested in the global structure of dSphs and will neglect their cold hearts. In addition, in order to keep the number of free parameters to a minimum, we assume that both, the stellar components and the dark matter cores are isotropic with negligible anisotropy effects (Salucci et al. 2012).

Adopting a central density $\rho(r=0) = \rho_0$, the radial density distribution $\rho(r)$ of an isothermal halo in hydrostatic equilibrium is determined by

$$\sigma_0^2 \frac{d \ln \rho}{dr} = - \frac{GM(r)}{r^2} \quad (3)$$

Here σ_0 is the dark matter velocity dispersion and $M(r)$ is the cumulative dark matter mass inside radius r . The assumption of virial equilibrium might not always be valid (Kroupa 1997), especially for tidal dwarf galaxies (Wetzstein et al. 2007; Ploekinger et al. 2014) and strongly tidally affected dSphs like the Sagittarius dwarf spheroidal (Ibata et al. 1994; Kroupa 1997; Yang et al. 2014). Deviations from hydrostatic equilibrium might therefore help to identify those (mostly outer) regions of dwarf satellites, that are tidally interacting with the host galaxy. The thick grey line in the upper left and right panels of figure 1 shows the density distribution and logarithmic slope $d \ln \rho / d \ln r$, respectively, of a non-singular isothermal sphere with finite ρ_0 . Inside the core radius that for an isothermal sphere is defined as

$$r_c^2 = \frac{9\sigma_0^2}{4\pi G\rho_0} \quad (4)$$

the dark matter density distribution is roughly flat. Note however that $\rho(r)$ is not exactly constant. This is due to the fact that, in equilibrium, the pressure gradient $\sigma^2 d\ln(\rho)/dr$ has to balance the gravitational force $GM(r)/r^2$. One might consider this a negligible effect for $r < r_c$. It is however precisely this small density gradient that determines the density distribution of the embedded stellar component.

Let us therefore now include a non self-gravitating, isothermal stellar component, as observed for dSphs. The stars then represent direct tracers of the underlying dark matter potential. It is unlikely that dSphs started that way. Obviously, the gas clouds from which the stars formed, were self-gravitating (Burkert & Hartmann 2013; Nipoti & Binney 2014). A low star formation efficiency, combined with strong galactic winds and ram pressure stripping might however have removed most of the baryons before they could condense into stars. This conclusion is also supported by the low metallicities of dSphs (Dekel & Silk 1986). If the galactic outflow was violent enough, in addition to leaving behind a non self-gravitating stellar system, it could also have reshaped an initially cuspy dark halo, generating a core (e.g. Navarro et al. 1996; Teyssier et al. 2013).

As both, the stars and the dark matter particles move inside the same joint gravitational potential their density distributions are coupled:

$$\sigma_*^2 \frac{d\ln \rho_*}{dr} = -\frac{GM(r)}{r^2} = \sigma_0^2 \frac{d\ln \rho}{dr}, \quad (5)$$

Here $\rho(r)$, ρ_0 and σ_0 are the density distribution, the central density and the velocity dispersion of the dark halo, respectively. $\rho_*(r)$ and σ_* correspond to the density distribution and velocity dispersion of the stellar component. Equation 5 leads to

$$\rho_*(r) = A \times \rho^\kappa(r) \quad (6)$$

with

$$\kappa = \frac{\sigma_0^2}{\sigma_*^2} \quad (7)$$

A is a constant of integration that determines the total stellar mass. Equation 6 shows that it is indeed the dark matter density gradient that determines $\rho_*(r)$:

$$\frac{d\ln \rho_*}{d\ln r} = \kappa \frac{d\ln \rho}{d\ln r}. \quad (8)$$

The three dashed lines in the upper panels of figure 1 show $\rho_*(r)$ for embedded stellar systems of our DIS model with velocity dispersions σ_*/σ_0 of 0.7, 0.5 and 0.25, corresponding to values κ of 2, 4 and 16, respectively. For $\kappa > 1.5$ the stellar density distribution decreases faster than r^{-3} in the outer region. In the academic limit that the DIS model holds for all r , the stellar system would have a finite mass, despite the fact that it is isothermal at all radii.

The middle, left panel of figure 1 shows the logarithm of the stellar density profile $\rho_*(r)$ and surface density distribution $\Sigma_*(r)$ (dashed and solid lines, respectively) as function of r^2 for $\kappa = 2, 4$, and 16. A Gaussian profile would be represented by a straight line and indeed fits the inner profiles in general quite well. The larger κ , the similar are the density and surface density distributions and the more do the profiles resemble a Gaussian.

Despite the fact that the dark matter core density is not precisely constant and by that equation 2 is not exactly valid we can still formally derive an approximate Gaussian scale length $a_* = -(d \ln \Sigma_*/dr^2)^{-1/2}$ by a least-squares linear fit of $\ln \Sigma_*$ versus r^2 within the innermost regions of the stellar component that we define as region, where Σ_* decreases by a factor e with respect to the central value. The middle right panel of figure 1 shows that a_*/r_c depends strongly on κ . Solving for ρ_0 in equation 2 and inserting it into equation 4 we find

$$\left(\frac{a_*}{r_c}\right) = 0.82 \left(\frac{\sigma_*}{\sigma_0}\right). \quad (9)$$

It is not clear whether this should work, given the fact that equation 2 was derived for a constant density core while we have argued that it is actually the dark matter density gradient that determines the stellar density distribution (equation 8). However the solid black line in figure 1 shows that equation 9 indeed provides an excellent fit to the actual data, derived from a numerical integration of the DIS model (red points).

In the lower left panel of figure 1 we test the validity of equation (2) as an estimation for the underlying dark halo density ρ_0 , given a_* and σ_* . If we write

$$\rho_0 = \eta_\rho \frac{3\sigma_*^2}{2\pi G a_*^2} \quad (10)$$

an analyses of the DIS model shows that η_ρ depends only on κ and in a way as shown by the solid black line. For $\kappa \geq 1$ a very good approximation is (red points)

$$\eta_\rho \approx 1.01(1 + 0.5 \exp[-(\kappa - 1)^{0.6}]). \quad (11)$$

As expected, for very cold stellar systems with $\kappa \gg 1$ the stellar system traces the innermost dark halo core with an almost constant density distribution. Here $\eta_\rho \approx 1$ and equation 2 provides a good estimate of ρ_0 . For kinematically hotter stellar systems, however, equation 2 is not valid anymore and the correction factor η_ρ has to be taken into account.

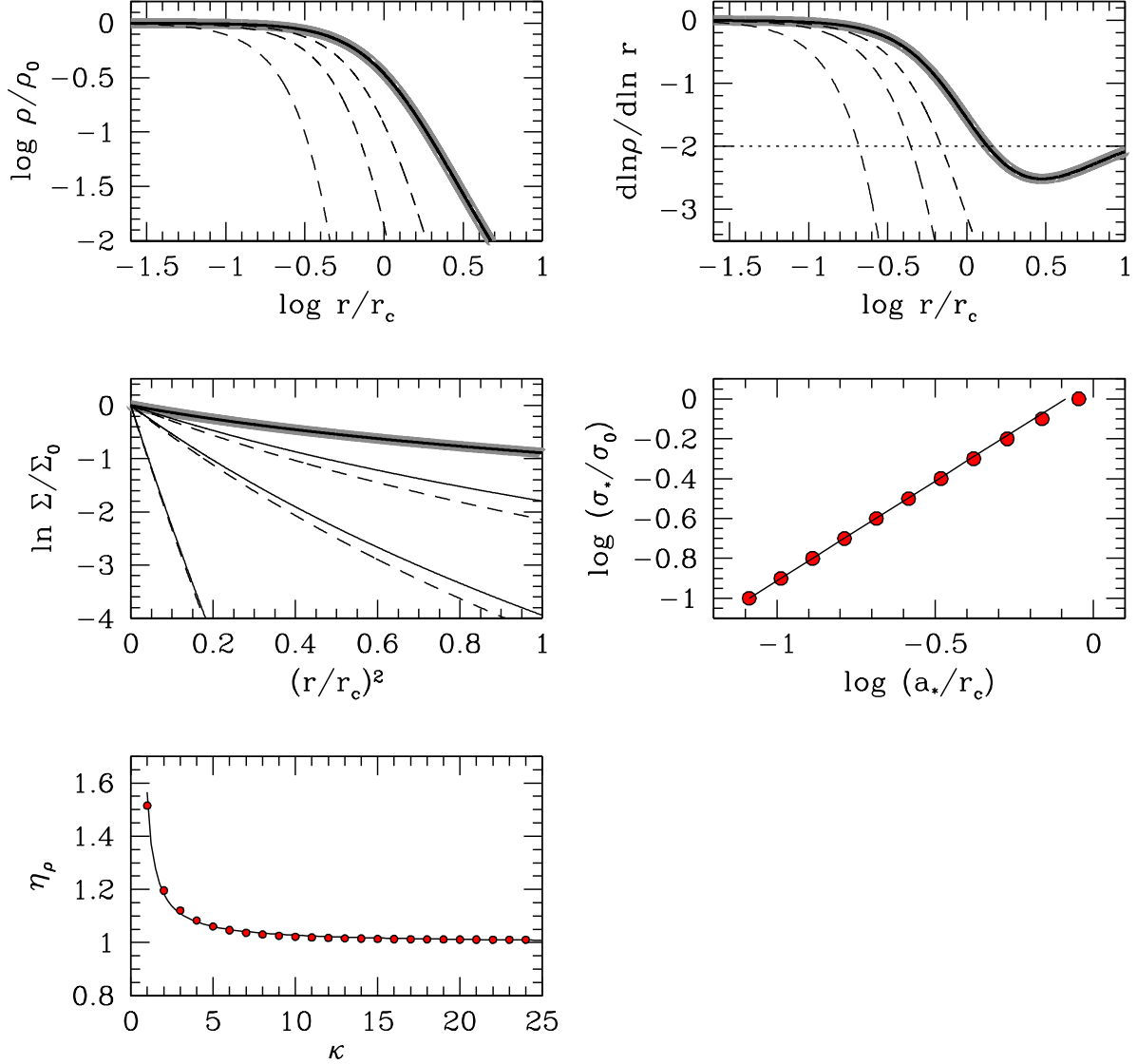


Fig. 1.— The thick lines in the upper left and right panels show the normalised density distribution and logarithmic density slope of an isothermal dark halo as function of radius. The dashed lines depict three embedded stellar systems with $\sigma_*/\sigma_0 = 0.7, 0.5$ and 0.25 , respectively. The thick line and the solid lines in the middle left panel show the surface density distribution of the dark halo and its three embedded stellar systems, respectively. Dashed lines in the middle left panel correspond to the normalised density distribution which is very similar to the surface density profile, especially for cold stellar systems. The red points in the middle, right panel show the correlation between σ_*/σ_0 of dark matter confined stellar systems as function of a_*/r_c , as determined by integrating the equations 3 and 6. The solid line shows equation 9. In the lower left panel the red dots show the correlation between the dark matter density parameter η_ρ (equation 10) and κ , derived by an integration of the DIS model. The solid line represents the empirical fit formula, equation 12.

3. King profiles and apparent extra-tidal components

Up to now we focussed on the innermost regions of dSphs that are sensitive to the central dark matter density. In order to gain information about the dark halo core radii and core masses we need to look at stellar traces further out. According to equation 6 very cold dSphs with $\kappa \gg 1$ populate regions that are deeply embedded in the dark halo core and that are therefore not good probes to explore the larger environment. One such example is Carina, shown in the upper left panel of figure 2. Carina can be fitted well by a Gaussian over most of the stellar body with a small change in slope $d \ln \Sigma_*/dr^2$ in the outermost region. In contrast, the stellar distribution of the much more extended Sculptor dSph (upper right panel of figure 2) deviates strongly from a Gaussian. The red solid lines in both figures show the surface density profiles of DIS systems following equations 3 to 7 with $\kappa = 3.3$ and $\kappa = 1.5$ for Carina and Sculptor, respectively. With respect to the dark matter component, the stellar system in Sculptor ($\sigma_* = 0.81\sigma_0$) is kinematically hotter than in Carina ($\sigma_* = 0.55\sigma_0$), leading to a more extended structure.

It turns out that the equations 3 to 7 lead to surface density distributions that fit all dSphs very well, even those with more complex, extended stellar components like Sculptor. This results from the fact that dSphs are in general observed to follow King profiles with different concentration parameters c . Here, $c = \log(r_{*,t}/r_{*,c})$, with $r_{*,t}$ and $r_{*,c}$ the tidal and core radius of the stellar system. The same is true for the projected surface density distributions of stellar systems in our DIS model. As an example, the solid lines in the left panel of figure 3 show three different stellar systems of our DIS model with κ values of 2.8, 1.4 and 1, respectively. The points show the corresponding best fitting King profiles which have concentrations of 0.6, 1.25 and 3.6, respectively. Note that this excellent fit hides a fundamental difference between DIS models and King models. Our stellar systems have constant velocity dispersions. They are part of a 2-component system, with the stars being embedded in a surrounding dark halo that has in general a different velocity dispersion than the stars. King models, instead, are one-component, self-gravitating particle systems that are sometimes also called truncated isothermal spheres. They are characterised by a special velocity distribution function that has been designed to fit stellar systems like globular clusters with sharp outer edges at r_t , generated as a result of tidal stripping. In order for such a sharp outer edge to exist, the velocity dispersion of the stars in the King model has to decrease with radius with $\sigma_* \rightarrow 0$ at r_t . Otherwise stars would be able to move beyond r_t . It is therefore surprising and at first not necessarily expected that the one-component King profiles with a completely different kinematics provide such a good fit to the stellar structure of our two-component DIS systems, over more than 4 orders of magnitude in $\ln \Sigma$.

A characteristic property of King models is that the surface density structure changes strongly for concentrations $1.2 \leq c \leq 2$ from a core with a steeply decreasing outer edge to a more extended structure. The DIS models follow this trend nicely with kinematically hotter stellar systems, characterised by smaller values of κ , corresponding to King models with larger c . In the transition regime, however, the best fitting King profiles are somewhat steeper than the stellar systems for $\ln \Sigma_*/\Sigma_{*,0} \leq -4$ (see the $c = 1.25$ profile in the left panel of figure 3). Interpreting such an extended

population of stars as extra-tidal, in this case, would be misleading. These stars are still deeply embedded and strongly bound to their dark halo. On the other hand, an extra-tidal component detected at that level in $\ln \Sigma_*/\Sigma_{*,0}$ in systems with concentrations $c < 1$ or $c > 2$ cannot be explained within the framework of our model and therefore might indeed represent a separate hot halo or even an extra-tidal component.

The right panel of figure 3 shows that there exists a tight correlation between the κ value of the DIS model and the King concentration parameter c (solid black line). The kinematically hotter the stellar system, i.e. the smaller κ , the more extended the stellar system and the larger c . The red points show the empirical relation

$$\log \kappa = 1.25 \exp(-1.72c) \quad (12)$$

which is an excellent fit to the data. Given a_* , σ_* and c one can now use the equations 9 to 12 and calculate the central density ρ_0 , velocity dispersion σ_0 and core radius r_c of the dark halo:

$$\begin{aligned} \log \left(\frac{r_c}{\text{pc}} \right) &= 0.088 + \log \left(\frac{a_*}{\text{pc}} \right) + 0.625 \exp(-1.72c) \\ \log \left(\frac{\sigma_0}{\text{km/s}} \right) &= 0.625 + \log \left(\frac{\sigma_*}{\text{km/s}} \right) + 0.625 \exp(-1.72c) \\ \log \left(\frac{\rho_0}{\text{M}_\odot/\text{pc}^3} \right) &= 2.04 + 2 \log \left(\frac{\sigma_*}{\text{km/s}} \right) - 2 \log \left(\frac{a_*}{\text{pc}} \right) \end{aligned} \quad (13)$$

4. The dark halo core properties of local Milky Way dSphs

As an application we now investigate the dark halo core properties of the 8 classical Milky Way dSphs (table 1), observed by Irwin & Hatzidimitriou (1995, IH95, see also Kormendy & Freeman 2014). IH95 determined their stellar surface density distribution with high enough resolution in order to derive King concentration parameters and determine the central scale lengths. IH95 also provide stellar velocity dispersions. The central Gaussian scale lengths a_{maj} were determined from the major axis surface brightness profiles, shown in figure 2 of IH95. These values are very close to the King core radii, summarized in Table 4 of IH95. Following IH95, a_* was then derived as the geometrical mean along the major and minor axis with $a_* = a_{maj} \times r_{c,g,IH}/r_{c,IH}$ where $r_{c,g,IH}$ and $r_{c,IH}$ is the stellar system's geometric mean and the major axis core radius, respectively, as determined by IH95.

Using the set of equations (13) we now can calculate the halo core parameters r_c , σ_0 and ρ_0 . The results are summarized in table 1. The upper left panel of figure 4 shows σ_* versus a_* (grey triangles) and σ_0 versus r_c (red points with error bars) for the 8 dSphs. Dark halo cores are hotter than their stellar systems with velocity dispersions in between 10-18 km/s and, on average,

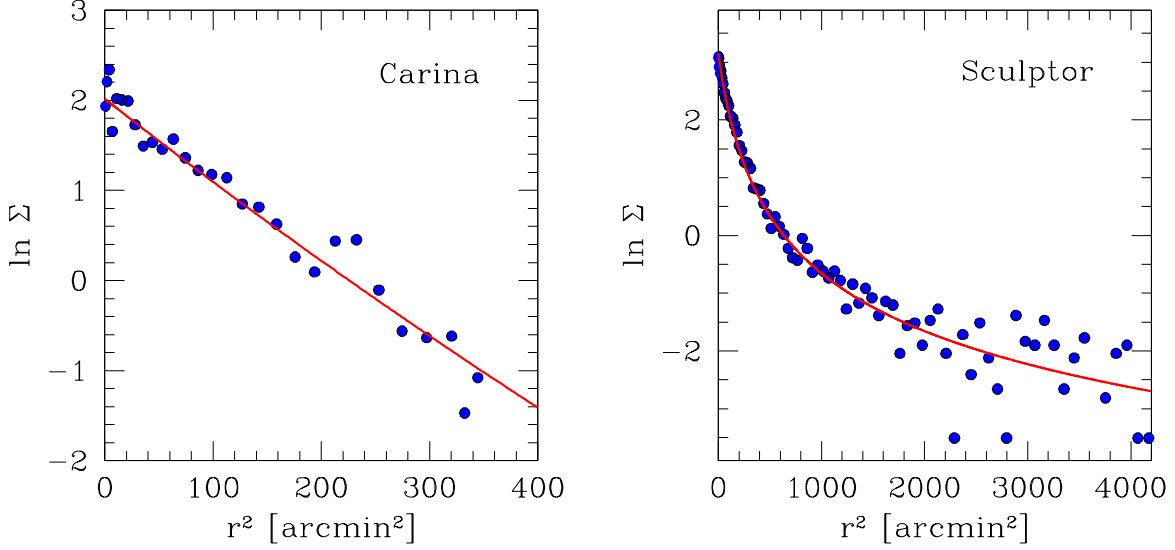


Fig. 2.— The blue points in each panel show the stellar surface density measurements of Irwin & Hatzidimitriou (1995) of the Milky Way dSphs Carina and Sculptor. DIS models (red lines) provide an excellent fit to the galaxies.

Table 1: Physical properties of the stellar and dark halo component of the 8 classical Milky Way dSphs (KF14, IH95).

	stellar component			dark matter component				
	a_* [pc]	σ_* [km/s]	c	r_c [pc]	σ_0 [km/s]	ρ_0 [$M_\odot \text{ pc}^{-3}$]	M_c [$10^7 M_\odot$]	M_{300} [$10^7 M_\odot$]
Carina	202	6.6	0.51	450	12.0	0.13	2.6	0.9
Draco	176	9.1	0.50	397	16.7	0.33	4.4	2.1
Leo I	221	9.2	0.58	460	15.6	0.22	4.6	1.6
Leo II	174	6.6	0.48	400	12.4	0.18	2.4	1.2
UMi	211	9.5	0.51	470	17.3	0.25	5.6	1.9
Fornax	705	11.7	0.72	1310	17.7	0.035	17.3	0.4
Sextans	400	7.9	0.98	641	10.3	0.053	3.0	0.5
Sculptor	189	9.2	1.12	286	11.4	0.33	1.7	1.5

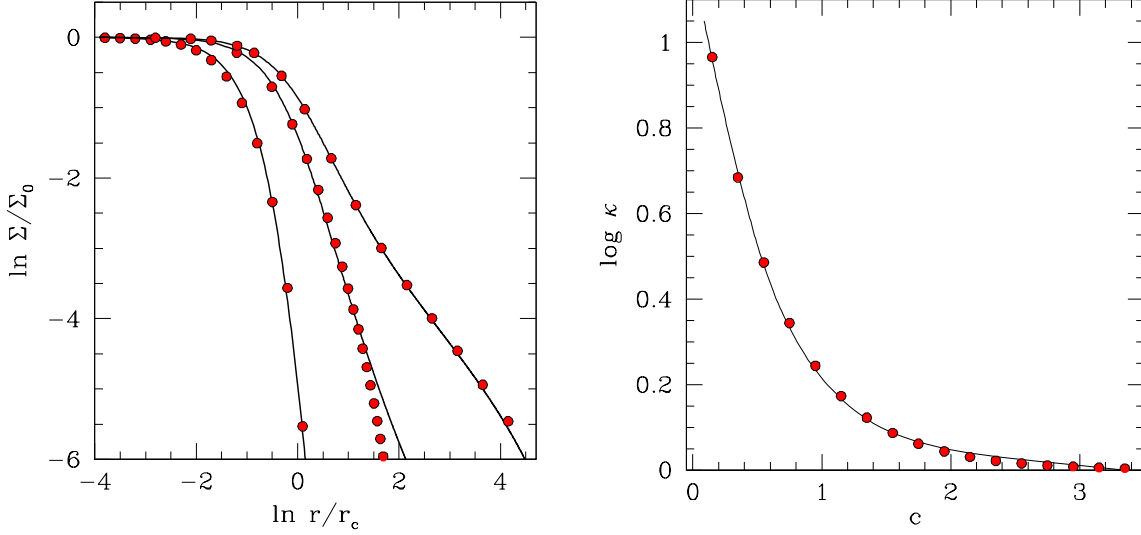


Fig. 3.— The left panel compares the normalised surface density distribution of three characteristic King profiles (red points) with different concentrations $c=0.6$ (innermost contour), 1.25 (middle) and 3.6 (outer contour) with the stellar surface density distribution of our DIS model (solid lines). Note the apparent “extra-tidal” stellar component for the profile with $c = 1.25$. The solid line in the right panel shows the correlation between the κ values of the DIS model and the concentration of the best fitting King profile. The red points show to the empirical fit formula, equation 11.

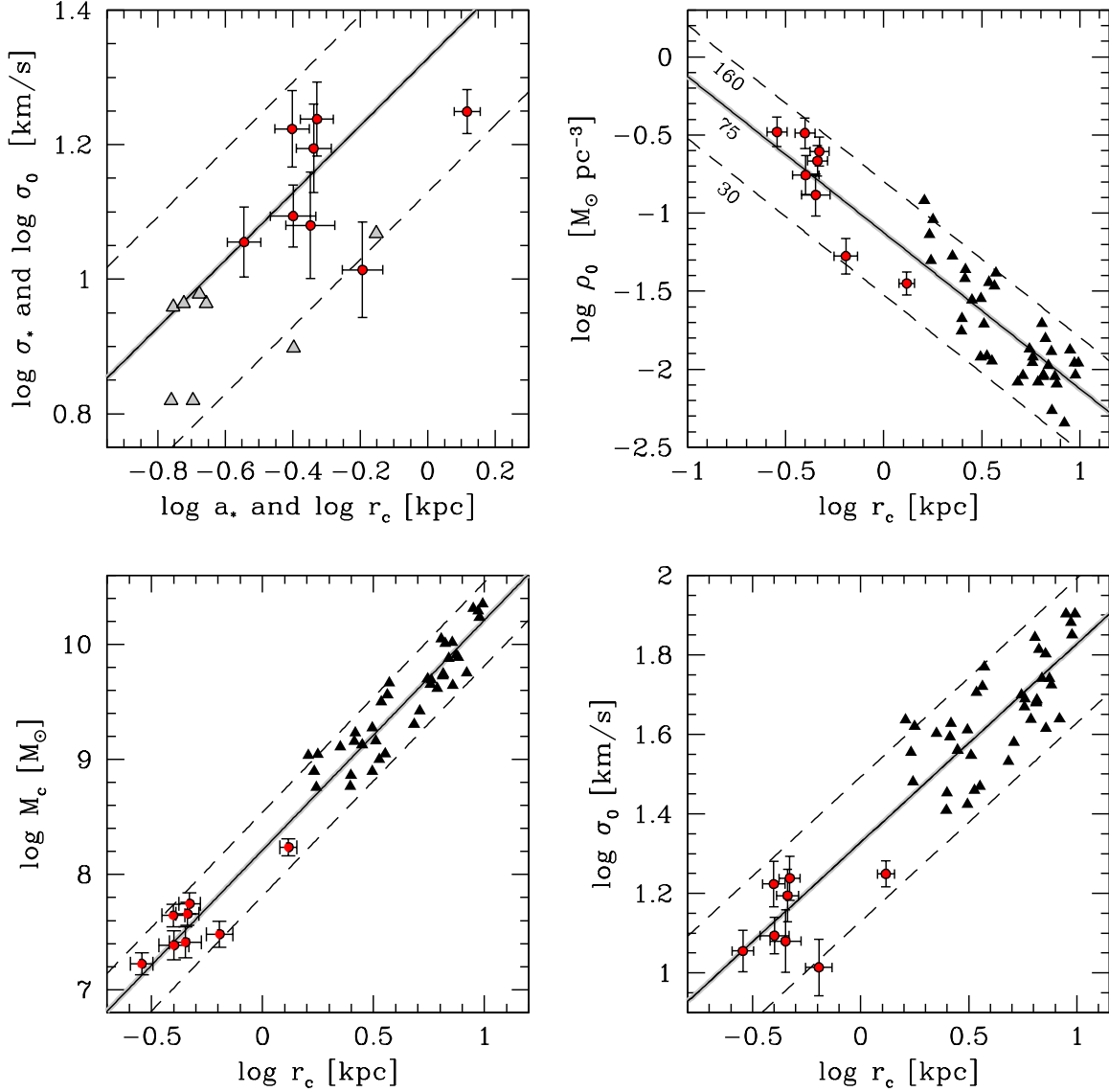


Fig. 4.— The grey triangles in the upper left panel show the stellar velocity dispersion σ_* versus the central stellar scale length a_* of the 8 classical Milky Way dSphs. Red points with errorbars depict the corresponding dark halo velocity dispersion σ_0 versus the halo core radius r_c . The red points in the upper right and lower left and right panels show the correlation of r_c with the dark halo central densities ρ_0 , core masses M_c and velocity dispersions σ_0 , respectively. Black triangles depict the core properties of more massive galaxies. The thick grey line in all four panels corresponds to the dark halo core scaling relation $\langle \rho_0 r_c \rangle = 75 M_\odot \text{ pc}^{-2}$ that fits all galaxies very well. The 2 dashed lines show the observed spread with the upper and lower limit corresponding to core surface densities of 30 and 160 $M_\odot \text{ pc}^{-2}$, respectively.

$\sigma_0 \approx 1.6\sigma_*$, corresponding to $\kappa \approx 2.56$. The halo core radii lie in the range of 290 pc to 1.3 kpc. On average, $r_c \approx 1.9a_*$. Donato et al. (2004) analysed a sample of high-resolution rotation curves of 25 disk galaxies and determined independently the disk scale lengths r_d and dark matter core radii. They found that both radii are strongly correlated with $r_d \approx 2.4r_c$. It is remarkable that the ratio between the stellar scale length and the dark halo scale length is the same (of order 2) in very different galactic systems over a large range of mass. The origin is still unclear and might provide further insight into the mechanisms that lead to dark matter cores.

The upper right panel of figure 4 shows the dark halo central surface densities ρ_0 as function of r_c . Typical values are $0.2 \text{ M}_\odot \text{ pc}^{-3}$ with a range of $0.03 - 0.3 \text{ M}_\odot \text{ pc}^{-3}$. It has been argued that dark halo cores follow a universal scaling relation with constant core surface density $\langle \rho_0 r_c \rangle$ (e.g. Athanassoula et al. 1987; Burkert 1995; Salucci & Burkert 2000; Kormendy & Freeman 2004; de Blok et al. 2008; Gentile et al. 2009; Donato et al. 2009; Kormendy & Freeman 2014, see however Saburova & del Popolo 2014). KF14 find that this scaling relation holds over more than 18 magnitudes in M_B . The black triangles in the upper right panel and in both lower panels of figure 4 show the core properties of galaxies, compiled from the literature by KF14 (see the list of references for the original data in table 1 of KF14). The core surface densities of all galaxies lie in a narrow range of $30 \text{ M}_\odot/\text{pc}^2 \leq \langle \rho_0 r_c \rangle \leq 160 \text{ M}_\odot/\text{pc}^2$ (dashed lines). The 8 Milky Way dSphs fall precisely into this regime, despite the fact that their r_c are on average a factor 6 smaller with ρ_0 being a factor of 6 larger. The lower left panel of figure 4 shows the dSph core masses, which for non-singular isothermal spheres are

$$M_c \equiv 2.17 \times \rho_0 r_c^3 = 162.75 \left(\frac{\langle \rho_0 r_c \rangle}{75 \text{ M}_\odot/\text{pc}^2} \right) \left(\frac{r_c}{\text{pc}} \right)^2 \text{ M}_\odot \quad (14)$$

The core masses cover a range of one order of magnitude with masses in between (see table 1) $1.7 \times 10^7 \leq M_c \leq 1.7 \times 10^8 \text{ M}_\odot$. The expected correlation between M_c and r_c (equation 14) is drawn for $\langle \rho_0 r_c \rangle = 30, 75$ and $160 \text{ M}_\odot \text{ pc}^{-2}$, together with the core masses of more massive galaxies. The dSphs follow the same core mass scaling relations as massive galaxies with the same spread. Finally, the lower right panel shows again σ_0 versus r_c . Now we compare the dSphs with the more massive galaxies. Both follow the same universal scaling relation $\sigma_0^2 \times r_c^{-1} = 0.45_{-0.27}^{+0.51} (\text{km/s})^2 \text{ pc}^{-1}$, again with precisely the same spread.

5. The origin of a common mass and length scale for dark matter cores

Strigari et al. (2008) proposed that all dSphs of the Milky Way have the same total dark matter mass $\log(M_{300}/\text{M}_\odot) = 7.0_{-0.4}^{+0.3}$, contained within a radius of 300 pc. The origin of a universal and constant mass might at first appear surprising, given the fact that the core masses are a strong function of core size (equation 14). Note however that M_c is measured within r_c whereas M_{300} is the mass within a fixed radius 300 pc that can be smaller or larger than r_c . The question still arises

why there should exist such a universal radius r_u , inside which halo cores have the same mass M_u and what determines this radius. In addition, adding Andromeda dSphs, Collins et al. (2014) find outliers that are not consistent with the Strigari et al. mass which indicates that the situation can be more complex.

Ogiya et al. (2014) discussed a possible connection between the existence of a universal mass scale and the universal core surface density of dSphs. Following Ogiya et al. (2014), let us now explore this question within the context of the DIS model. We start with a population of dSphs that has a common core surface density $\langle \rho_0 r_c \rangle$. Given r_c , one can determine ρ_0 and with equation (4) σ_0 . An integration of equation (3) then gives the complete density profile and by this M_u . The horizontal lines in figure 5 show M_{300} as function of r_c for the typical surface densities $\langle \rho_0 r_c \rangle = 75^{+75}_{-40} \text{ M}_\odot \text{ pc}^{-2}$ of the Milky Way dSphs. Interestingly, M_{300} is not continuously increasing with r_c but instead has a maximum at the point where it crosses the correlation between halo core mass and core radius (vertical lines). This point also corresponds to the adopted characteristic scale length $r_u = 300 \text{ pc}$. The blue and red points in figure 5 show the dSph’s M_{300} and M_c , respectively. We added 10 dSphs from table 1 of Strigari et al. (2008) with given M_{300} and King radii r_{king} (blue triangles). The halo core radii are not known for this sample. For our joint sample we find on average $r_c \approx 2.3 r_{king}$ which was used in figure 5 in order to estimate r_c for the dSphs with unknown core radii. The red points follow the expected correlation between core mass and core radius (vertical solid and dotted lines). The M_{300} masses however show no such correlation with r_c but instead are roughly constant. Table 1 summarizes the M_{300} values of our sample of Milky Way dSphs. With on average $M_{300} = 1.3 \pm 0.6 \times 10^7 \text{ M}_\odot$ they are in excellent agreement with Strigari et al. (2008).

The horizontal lines in figure 5 however show also that M_{300} is not precisely constant but should depend on the halo core radius. This is true for any adopted radius r_u . Within the framework of the DIS model there exists no universal radius r_u inside which M_u is constant for a population of dSphs with given core surface density. It is however interesting that M_u reaches a maximum for halos with core radii $r_c = r_u$. This is true for any adopted length scale r_u . As M_u is very insensitive to r_c in the flat vicinity of this maximum, all dSphs with core radii in this regime would show very similar M_u values, which is exactly what we observe for the Milky Way’s dSphs. The best choice of r_u therefore is the average logarithmic core radius of a given sample of dSphs with universal core surface densities. M_u is then the mass within a dark halo core with $r_c = r_u$ (equation 14):

$$\log r_u = \frac{1}{N} \sum_{i=1}^N \log r_{c,i} \quad (15)$$

$$M_u = 2.17 \langle \rho_0 r_c \rangle r_u^2$$

with N the number of dSphs and $r_{c,i}$ the core radius of galaxy i . The origin of a maximum for $r_c = r_u$ can be easily understood. For $r_c > r_u$ the core radius is larger than the region sampled by

r_u and the density is roughly constant with a value $\rho_0 \sim 1/r_c$ due to the assumption of a constant core surface density. The enclosed mass is then $M_u \sim \rho_0 r_u^3 \sim 1/r_c$ leading to M_u decreasing with increasing r_c . For $r_c < r_u$ the region is larger than the core and extends out to radii where the dark matter density distribution begins to decrease. To first order we can approximate M_u now as the mass of a constant density core $\rho(r) = \rho_0$ for $r \leq r_c$ plus the mass of an envelope with a power-law density distribution $\rho = \rho_0 \times (r_c/r)^2$. As $\rho_0 \sim 1/r_c$ we get $M_u \sim r_c^2(r_u/r_c - 2/3)$ which is a continuously increasing function with increasing r_c .

Applying equation 15 to our sample of dSphs we find $r_u = 400 \pm 100$ pc and with $\langle \rho_0 r_c \rangle = 75 \text{ M}_\odot \text{ pc}^{-2}$ get $M_u = 2.4 \pm 1.4 \times 10^7 \text{ M}_\odot$, in good agreement with Strigari et al. (2008). If the population has a large spread in r_c we also expect to find outliers, populating the wings of the distribution further away from the maximum with smaller masses M_u . This might explain the detection of outliers in Andromeda’s system of dSphs (Collins et al. 2014).

6. Summary and conclusions

Motivated by the conjecture that dSphs are isothermal stellar systems, embedded in isothermal dark matter cores we investigated the structure of two particle systems with constant but different velocity dispersions, in virial equilibrium within their joint gravitational potential. Note that here the main objective was not to demonstrate that dark matter cores are isothermal and isotropic and it certainly has to break down outside of some radius (Burkert 1995). We worked with this assumption because it is the most simple model of a halo core with the least number of free parameters. Of course, the fact that we find solutions that fit the observations very well is promising. But it is not a proof due to the fact that a fine tuned radial distribution of anisotropy, coupled with a properly chosen gradient in velocity dispersion could always lead to similar cored density profiles.

So far DIS systems have not been investigated in details in the literature. We demonstrate that the surface density distributions of the non self-gravitating stellar system can show a rich variety of profiles. They can formally be fitted by King profiles despite the fact that the DIS model consists of two isothermal components in contrast to the one-component, non-isothermal King model. We find that the stellar systems in the DIS models have steeply decreasing outer edges at $r = r_t$, especially for high values of κ , not because they are tidally limited but because they are deeply embedded within the inner core regions of their dark halo. This is in contrast to the real one-component King model where r_t is the Roche radius, where the gravitational potential of the host galaxy begins to dominate. In addition, DIS systems have projected velocity dispersion profiles that remain constant all the way till r_t . One-component King systems, on the other hand, would show outer velocity dispersion profiles that decrease towards $\sigma_* = 0$ at r_t . Measurements of the stellar velocity dispersion of dSphs close to their tidal radius therefore could help to distinguish tidally truncated one-component systems without confining dark halos (Yang et al. 2014) from those where r_t is a result of strong dark matter confinement. This is also important, as the outer radii r_t of satellite galaxies, interpreted as a tidal radius, have been used in order to gain information

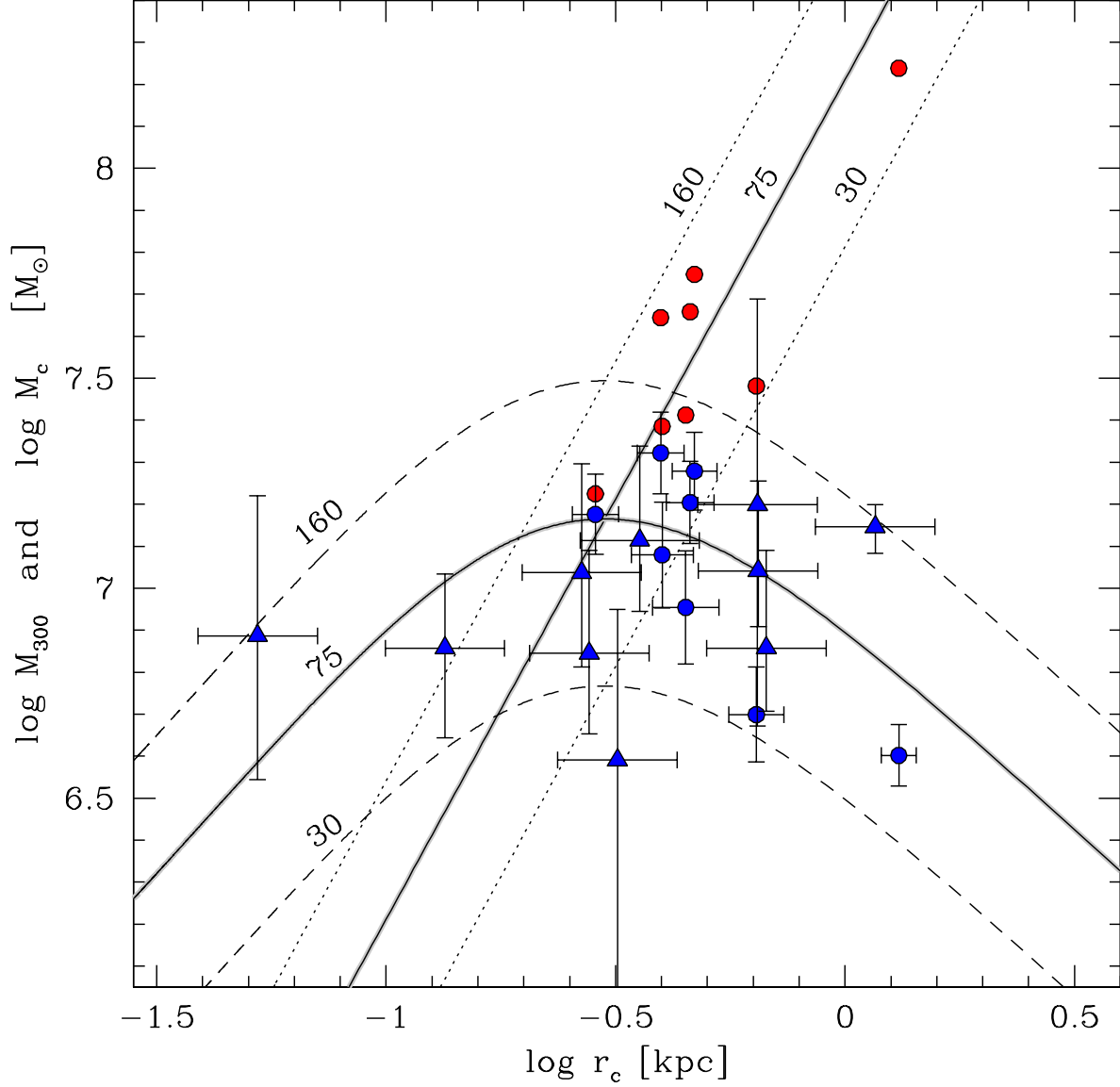


Fig. 5.— Red and blue points show the dSph’s core masses M_c and masses M_{300} within a fixed radius $r_u = 300$ pc, summarized in table 1. Blue triangles show additional dSphs taken from table 1 of Strigari et al. (2008). The red points follow the core scaling relations $\rho_0 \times r_c = 75^{+85}_{-40} \text{ M}_\odot \text{ pc}^{-2}$, observed for massive galaxies (solid and dotted lines). The second set of solid and dashed lines with a maximum at $r_c = 300$ pc shows the predicted relationship between M_{300} and r_c for halos with the same core surface densities. All lines are labeled according to their core surface density in units of $[\text{M}_\odot \text{ pc}^{-2}]$.

about the satellite’s orbital parameters or the dark halo mass distribution of the host galaxy (e.g. Pasetto et al. 2011). Our analyses instead shows that r_t measures the radius of the satellite’s dark halo core and therefore does not contain information about the location of the tidal radius.

That r_t traces the dark halo’s core radii follows from the fact that the dSphs on average have $\kappa \approx 2.6$. r_t is close to the point, where the logarithmic density gradient $d \ln \rho_*/d \ln r$ begins to decrease faster than -3 which, according to equation 8, then corresponds to a dark halo density gradient of $d \ln \rho/d \ln r = -3/\kappa = -1.2$. The upper right panel of figure 1 shows that this slope is close to the core radius r_c of the dark matter halo. It is not clear yet, whether this is a coincidence or whether the processes that generated the dark halo cores and their non-self gravitating stellar tracer component naturally lead to such a configuration (Dekel & Woo 2003).

For DIS systems, the central Gaussian scale length a_* , the velocity dispersion σ_* and the concentration c of the stellar component completely specify the dark halo core parameters ρ_0 , σ_0 and r_c . We determined these parameters for 8 dSphs of the Milky Way and find that their dark halos have the same core surface densities $\rho_0 \times r_c = 75^{+85}_{-45} \text{ M}_\odot \text{ pc}^{-2}$ as more massive galaxies, with exactly the same spread. This is very puzzling as dSphs have a different structure and live in very different environments. The origin of dark matter cores is still not well understood. Suggestions range from gravitational interaction with the baryonic component (e.g. Navarro et al. 1996; El-Zant et al. 2001; Goerdt et al. 2010; Inoue & Saitoh 2011; Ogiya & Mori 2011; Pontzen & Governato 2012; Governato et al. 2012; Teyssier et al. 2013; Gritschneider & Lin 2013; Ogiya & Mori 2014; Ogiya et al. 2014) to a non-standard primordial power spectrum (Zentner & Bullock 2002; Polisensky & Ricotti 2014), warm dark matter (e.g. Lovell et al. 2014), other intrinsic properties of dark matter like self-interaction and self-annihilation (e.g. Spergel & Steinhardt 2000; Burkert 2000; Loeb & Weiner 2011; Elbert et al. 2014) or modifications of Newtonian dynamics (e.g. Milgrom 1983; Kroupa 2012). Whatever the mechanisms, considerable fine tune is required in order to generate a universal core scaling relation over more than 18 orders of magnitudes in blue magnitude M_B with exactly the same spread.

Adopting a constant core surface density, M_c depends strongly on r_c . Focussing however on a fixed radius r_u , the enclosed mass M_u shows a different dependence on halo core radius, with a maximum at $r_c = r_u$. All halos with core radii in the vicinity of this maximum should therefore show similar values of M_u which could explain the observations of Strigari et al. (2008). The best choice of r_u is therefore dependent on the dSph’s distribution of r_c . There does however not exist a universal mass scale M_u that is independent of r_c . Smaller values of M_u are expected for outliers with core radii that are very different from r_u . Turning this argument around, if such a universal mass would exist, independent of r_c , it would be a clear signature that dark halo cores are not isothermal.

As the core radii of dSphs are small, their core densities have to be high in order for the core surface density to remain constant. This should shield dSphs efficiently against the tidal forces of their host galaxies. Adopting a constant rotation curve v_{rot} , the Milky Way’s mean density within

a given radius r is

$$\langle \rho_{MW} \rangle = \frac{3v_{rot}^2}{4\pi Gr^2} = 2.7 \left(\frac{v_{rot}}{220 \text{ km/s}} \right)^2 \left(\frac{\text{kpc}}{r} \right)^2 \text{ M}_{\odot} \text{ pc}^{-3} \quad (16)$$

The stellar system in dSphs would be tidally affected if $\langle \rho_{MW} \rangle > \rho_0 \approx 0.2 \text{ M}_{\odot} \text{ pc}^{-3}$ which requires orbital pericenters of order a few kpc, which is very unlikely. dSphs therefore should be strongly shielded from any tidal affects by their deep dark matter potential wells and should survive as satellites of the Milky Way for a long time to come. However extra-tidal debris has been reported in some dSphs (IH95 Walcher 2003; Majewski et al. 2005; Battaglia et al. 2012). We discussed in section 3 that the DIS model in a certain concentration regime indeed leads to profiles that are somewhat more extended than the best fitting King profiles. This could be mis-interpreted as a tidal component. Strong evidence for tidal interactions would however represent a real challenge for the existence of a shielding dark halo, opening the door for alternative ideas (Milgrom 1983; Yang et al. 2014).

This work was supported by the cluster of excellence "Origin and Structure of the Universe". I thank my CAST group at the University Observatory, Munich for inspiring discussions and suggestions. Special thanks also go to Edvige Corbelli, Avishai Dekel, Ken Freeman, Pavel Kroupa, Go Ogiya, Jerry Ostriker, Paolo Salucci and David Spergel for interesting discussions and a careful reading of the manuscript. Finally I would like to thank the Harvard Center for Astrophysics for support, lively discussions and an infinite supply of coffee that was essential and the driver for finishing this paper.

REFERENCES

- Athanassoula, E., Bosma, A. & Papaioannou, S. 1987, *A&A*, 179, 23
- Battaglia, G., Irwin, M., Tolstoy, E., de Boer, T. & Mateo, M. 2012, *ApJ*, 761, L31
- Boylan-Kochlin, M., Bullock, J. S. & Kaplinhat, M. 2011, *MNRAS*, 415, L40
- Burkert, A. 1995, *ApJ*, 447, L25
- Burkert, A. 1997, *ApJ*, 474, L99
- Burkert, A. & Hartmann, L. 2013, *ApJ*, 733, 10
- Burkert, A. 2000, *ApJ*, 534, L143
- Burkert, A. et al. 2014, *ApJ*, 725, 232
- Carignan, C. & Freeman, K. C. 1985, *ApJ*, 294, 494

- Collins, M. L. M. et al. 2014, *ApJ*, 783, 14
- Corbelli, E., Thilker, D., Zibetti, S., Giovanardi, C. & Salucci, P. 2014, *A&A*, 572, 18
- de Blok, W. J. G., McGaugh, S. S. & Rubin, V. C. 2001, *AJ*, 122, 2396
- de Blok, W. J. G., Walter, F. et al. 2008, *AJ*, 136, 2648
- de Blok, W. J. G. 2010, *Adv. Astr.*, 2010, 789293
- Dekel, A. & Silk, J. 1986, *ApJ*, 303, 39
- Dekel, A., Devor, J. & Hetzroni, G. 2003a, *MNRAS*, 341, 326
- Dekel, A. & Woo, J. 2003b, *MNRAS*, 344, 1131
- Dib, S., Bell, E. & Burkert, A. 2006, *ApJ*, 638, 797
- Donato, F., Gentile, G. & Salucci, P. 2004, *MNRAS*, 353, L17
- Donato, F. et al. 2009, *MNRAS*, 397, 1169
- Dubinski, J. & Carlberg, R. G. 1991, *ApJ*, 378, 496
- Elbert, O. D. et al. 2014, submitted to *MNRAS*, arXiv:1412.1477
- El-Zant, A., Shlosman, I. & Foffman, Y. 2001, *ApJ*, 560, 636
- Flores, R. A. & Primack, J. R. 1994, *ApJ*, 427, L1
- Gentile, G., Famaey, B., Zhao, H. & Salucci, P. 2009, *Nature*, 461, 627
- Goerdt, T., Moore, B., Read, J. I. & Stadel, J. 2010, *ApJ*, 777, 119
- Goerdt, T., Burkert, A. & Ceverino, D. 2014, submitted, arXiv: 1307.2102
- Governato, F. et al. 2012, *MNRAS*, 422, 1231
- Gritschneider, M. & Lin, D. N. C. 2013, *ApJ*, 765, 38
- Ibata, R. A., Gilmore, G. & Irwin, M. J. 1994, *Nature*, 370, 194
- Ibata, R. A. et al. 2013, *Nature*, 7430, 62
- Inoue, S. & Saitoh, T. R. 2011, *MNRAS*, 418, 2527
- Irwin, M. & Hatzidimitriou, D. 1995, *MNRAS*, 277, 1354
- Jungman, G., Kamionkovski, M. & Griest, K. 1996, *Phys. Rep.*, 267, 195
- King, I. R. 1966, *AJ*, 71, 64

- Kormendy, J. & Freeman, K. C. 2004, in IAU Symposium 220, Dark Matter in Galaxies, ed. S. D. Ryder, D. J. Pisano, M. A. Walker & K. C. Freeman (San Francisco: ASP), 377
- Kormendy, J. & Freeman, K. C. 2014, submitted to ApJ, arXiv:1411.2170
- Kroupa, P. 1997, *New Astronomy*, 2, 139
- Kroupa, P., Theis, C. & Boily, C. M. 2005, *A&A*, 431, 517
- Kroupa, P. et al. 2010, *A&A*, 523, 22
- Kroupa, P. 2012, *PASA*, 29, 395
- Loeb, A. & Weiner, N. 2011, *Physical Review Letters*, 106, 171302
- Lovell, M. R., Frenk, C. S., Eke, V. R., Jenkins, A., Gao, L. & Theuns, T. 2014, *MNRAS*, 439, 300
- Majewski, S. R. et al. 2005, *AJ*, 130, 2677
- Majewski, S. R. et al. 2013, *ApJ*, 777, L13
- Maller, A. H. & Dekel, A. 2002, *MNRAS*, 335, 487
- Milgrom, M. 1983, *ApJ*, 270, 365
- Moore, B. 1994, *Nature*, 370, 629
- Moore, B., Quinn, T., Governato, F., Stadel, J. & Lake, G. 1999, *MNRAS*, 310, 1147
- Navarro, J. F., Eke, V. & Frenk, C. S. 1996, *MNRAS*, 283, 72
- Navarro, J. F., Frenk, C. S. & White, S. D. M. 1997, *ApJ*, 490, 493
- Nipoti, C. & Binney, J. 2014, *MNRAS*, 446, 1820
- Ogiya, G. & Mori, M. 2011, *ApJ*, 736, L2
- Ogiya, G. & Mori, M. 2014, *ApJ*, 793, 46
- Ogiya, G., Mori, M., Ishiyama, T & Burkert, A. 2014, *MNRAS*, 440, 71
- Ogiya, G. & Burkert, A. 2015, *MNRAS*, 446, 2363
- Oh, S.-H., de Blok, W. J. G., Brinks, E., Walter, F. & Kennicutt, R. C., Jr. 2011, *AJ*, 141, 193
- Ostriker, J. P. & Peebles, P. J. E. 1973, *ApJ*, 186, 467
- Pasetto, S., Grebel, E. K., Berczik, P., Chiosi, C. & Spurzem, R. 2011, *A&A*, 525, 99
- Ploekinger, S., Recchi, S., Hensler, G. & Kroupa, P. 2014, accepted for publication in *MNRAS*, arXiv: 1412.3450

- Polisensky, E. & Ricotti, M. 2014, MNRAS, 437, 2922
- Pontzen, A. & Governato, F. 2012, MNRAS, 421, 3464
- Primack, J. R. 2009, in Proceedings of the 8th UCLA Symposium, AIP Conf. Proc., 1166, 3
- Saburova, A. & del Popolo, A. 2014, MNRAS, 445, 3512
- Salucci, P. & Burkert, A. 2000, ApJ, 537, L9
- Salucci, P. et al. 2012, MNRAS, 420, 2034
- Spergel, D. N. & Steinhardt, P. J. 2000, Physical Review Letters, 84, 3760
- Steigman, G. & Turner, M. S. 1985, Nuclear Physics B, 253, 375
- Strigari, L. E. et al. 2008, Nature, 454, 1096
- Teyssier, R., Pontzen, A., Dubois, Y. & Justin, I. R. 2013, MNRAS, 429, 3068
- Walcher, C. J., Fried, J. W., Burkert, A. & Klessen, R. S. 2003, A&A, 406, 847
- Walker, M. G., Mateo, M., Olszewski, E. W., Peñarrubia, J., Wyn, E. N. & Gilmore, G. 2009, ApJ, 704, 1274
- Wetzstein, M., Naab, T. & Burkert, A. 2007, MNRAS, 375, 805
- White, S. D. M. & Negroponte, J. 1982, MNRAS, 201, 401
- Yang, Y., Hammer, F., Fouquet, S., Flores, H., Puech, M., Pawlowski, M. S. & Kroupa, P. 2014, submitted to MNRAS, arXiv:1405.2071
- Zentner, A. R. & Bullock, J. S. 2002, Phys. Rev. D, 66, 043003